

Equivariant representations for molecular Hamiltonians and N -center atomic-scale properties

Jigyasa Nigam,^{1,2} Michael Willatt,¹ and Michele Ceriotti^{1,2,*}

¹*Laboratory of Computational Science and Modeling, Institute of Materials,
École Polytechnique Fédérale de Lausanne, 1015 Lausanne, Switzerland*

²*National Centre for Computational Design and Discovery of Novel Materials (MARVEL),
École Polytechnique Fédérale de Lausanne, 1015 Lausanne, Switzerland*

Symmetry considerations are at the core of the major frameworks used to provide an effective mathematical representation of atomic configurations, that are then used in machine-learning models to predict the properties associated with each structure. In most cases, the models rely on a description of atom-centered environments, and are suitable to learn atomic properties, or global observables that can be decomposed into atomic contributions. Many quantities that are relevant for quantum mechanical calculations, however – most notably the Hamiltonian matrix when written in an atomic-orbital basis – are *not* associated with a single center, but with two (or more) atoms in the structure. We discuss a family of structural descriptors that generalize the very successful atom-centered density correlation features to the N -centers case, and show in particular how this construction can be applied to efficiently learn the matrix elements of the (effective) single-particle Hamiltonian written in an atom-centered orbital basis. These N -centers features are fully equivariant – not only in terms of translations and rotations, but also in terms of permutations of the indices associated with the atoms – and lay the foundations for symmetry-adapted machine-learning models of new classes of properties of molecules and materials.

I. INTRODUCTION

Most of the successful and widely used machine learning schemes that have been applied, over the past decade, to chemistry and materials aimed at learning molecular energies or interatomic potentials^{1–5}. As a consequence, the *representations* used to map atomic configurations into vectors of descriptors or features,^{6–14} to be used as inputs of the models, reflect some of the fundamental properties of the interatomic potential, such as the invariance to permutation between identical atoms, rigid rotation and inversion of the molecular structure, as well as the notions of locality and nearsightedness¹⁵. This latter, in particular, suggested to use atom-centered features that describe the arrangement of neighbors around a tagged atom. The number of neighbors considered simultaneously enumerates a hierarchy of ν -body representations, with increasing complexity and descriptive power. Notably, atom-centered representations have been used not only to build models of properties associated with an individual atomic center i , such as NMR chemical shieldings^{16–18}, but also to express global, extensive properties such as the molecular energy as a sum of atom-centered contributions.

More recently, symmetry-invariant models have been increasingly generalized to be imbued with *equivariant* behavior with respect to rotations and inversion,^{19–22}, addressing the need to construct data-driven models for atomic properties that have a structure more complicated than that of a scalar, such as dipole moments,^{23,24} polarizabilities,²⁵ and fields such as the charge²⁶ and on-top²⁷ densities. In the vast majority of cases, these equivariant representations

are still used together with atom-centered frameworks, that allow for superior transferability between systems of different size – the main limitation being connected with the finite range of the environment they can describe²⁸, unless they are combined with features specifically designed to capture the multi-scale nature of interactions²⁹.

While atom-centered descriptions are the most common in the construction of interatomic potentials, there are also examples in which the energy has been expanded as a sum of *pair* energies³⁰. Perhaps more importantly, there are several properties that are intrinsically associated with multiple atomic centers. J-couplings in NMR³¹, that describe the magnetic interaction between nuclear spins, are a typical example. Another example, that we will focus on in this work, involves the matrix elements of the electronic Hamiltonian (\hat{H}) when written in an atomic orbital basis. A classical example is that of tight-binding models³², in which the matrix elements of a minimal-atomic-basis Hamiltonian are parameterized in terms of interatomic distances and angles. Constructing data-driven models that match more closely explicit electronic structure calculations is an appealing approach to obtain improved semiempirical methods, and to access the many observables, such as optical excitations³³, that can be approximated based on the eigenvalues of an effective single-particle Hamiltonian. Furthermore, a machine-learned \hat{H} could also be used as inputs of the emerging family of ML models that predict molecular properties using matrix elements computed by explicit electronic-structure calculations^{34,35}.

Existing machine learning approaches that attempt to predict the molecular Hamiltonian do so in terms of an ad-hoc modification of the atom-centered features³⁶ or by devising pair features³⁷, that how-

* michele.ceriotti@epfl.ch

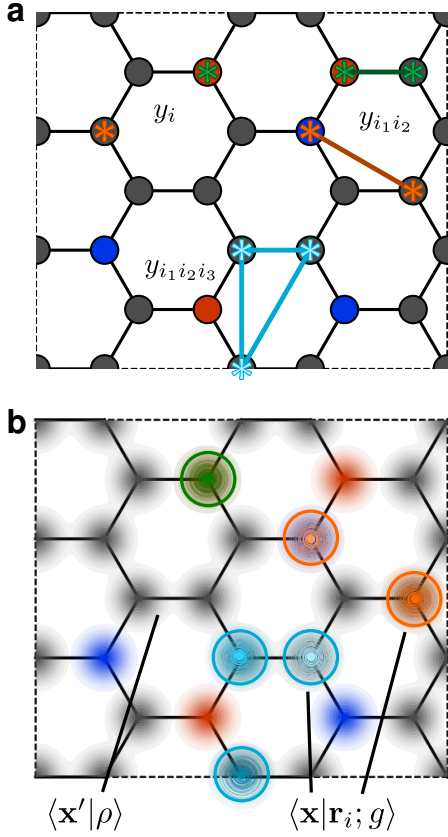


Figure 1: (a) A schematic depiction of the definition of N -centers quantities associated with an atomic configuration. (b) A representation of 1,2, and 3-centers clusters in terms of atom densities.

ever do not explicitly include the rotational symmetries and instead rely on data augmentation to incorporate them in the model. An interesting approach, recently proposed by Westermeyer and Maurer,³³ predicts an *invariant* pseudo-Hamiltonian matrix that has the correct eigenvalues, even though it does not need to bear any resemblance to the actual atomic orbital Hamiltonian.

To put the problem of learning these kinds of properties on a more solid mathematical footing, we introduce a symmetrized N -center representation that provides a natural, fully equivariant framework to learn properties that are associated with N atoms. We discuss its construction and its relationship to 1-center density correlation representations, and then demonstrate its use for the particular case of the two-center Hamiltonian. We show that the combination of atomic index and geometric equivariance incorporates naturally the symmetry considerations behind molecular orbital theory. As a result of the symmetry constraints, a small number of reference configurations suffice to achieve robust, accurate predictions of \hat{H} , that are competitive with state-of-the-art, deep-learning models despite using only linear or kernel regression.

II. N -CENTERS FEATURES

We address the problem of building a representation for atomistic properties that depend on the indices of several atoms, $y_{i_1 i_2 \dots}$ of a structure A (Figure 1). Atomic properties may be written as y_i , and properties associated with pairs of atoms as $y_{i_1 i_2}$. Models built to predict these properties should be equivariant with respect to changes in the atom labels: if we relabel the indices 1 and 2, respectively, as 7 and 9, equivariance requires that $y_1 \rightarrow y_7$, $y_2 \rightarrow y_9$, $y_{12} \rightarrow y_{79}$, $y_{221} \rightarrow y_{997}$, etc.

We may write a representation that aims to describe the structural features that determine the value of $y_{i_1 i_2 \dots}(A)$ as $\langle q | A_{i_1 i_2 \dots} \rangle$. We use the bra-ket notation that has been introduced in Refs. 13,38; the interested reader will find a thorough discussion in Section IV.A of Ref. 39. In short, the ket indicates the entity being represented (the N -centers tuple $A_{i_1 i_2 \dots}$), and we will supplement it with other indices that describe the nature and symmetry of the descriptors. The bra, instead, contains the (discrete or continuous) indices that enumerate the components of the feature vector associated with this entity. A linear model to predict $y_{i_1 i_2 \dots}$ can then be written as

$$\tilde{y}_{i_1 i_2 \dots}(A) = \sum_q \langle y | q \rangle \langle q | A_{i_1 i_2 \dots} \rangle. \quad (1)$$

It is clear that – in order for the prediction \tilde{y} to be equivariant with respect to permutation of indices – the features associated with $A_{i_1 i_2 \dots}$ must also be equivariant to changes in the atom labeling. In fact, the atom-centered features that underlie the vast majority of modern machine-learning interatomic potentials *are* equivariant with respect to the atom labelling: if we reverse the storage order of the atoms in a structure, the storage order of the various atomic contributions will also be reversed. Summing over the contributions to yield the *total* energy leads to a permutation-invariant model, and the equivariance of the underlying contributions is not usually given much emphasis.

A. Label-equivariant structural representation

We can write descriptors that fulfill atom-indices equivariant properties by “tagging” the selected atoms with an atom-centered function, e.g. a Gaussian $\langle \mathbf{x} | \mathbf{r}_i; g \rangle \equiv g(\mathbf{x} - \mathbf{r}_i)$. Each center can be associated with a separate function, so that the descriptor is indexed by $3N$ spatial coordinates, and the relative position of the atoms is encoded in the position of the Gaussian peaks. In order to express the relationship between the tagged centers and the rest of the structure, we can combine these functions with the overall atom density $\langle \mathbf{x} | \rho \rangle = \sum_j \langle \mathbf{x} | \mathbf{r}_j; g \rangle$ (Figure 1b), that

is invariant to permutations of the atoms labels

$$\begin{aligned} \langle \mathbf{x}_1; \mathbf{x}_2; \dots; \mathbf{x}_n; \mathbf{x}'_1; \mathbf{x}'_2; \dots; \mathbf{x}'_\nu | \rho_{i_1 i_2 \dots i_N}^{\otimes \nu} \rangle \equiv \\ \langle \mathbf{x}_1 | \mathbf{r}_{i_1}; g \rangle \langle \mathbf{x}_2 | \mathbf{r}_{i_2}; g \rangle \dots \langle \mathbf{x}_n | \mathbf{r}_{i_N}; g \rangle \times \\ \sum_{j_1} \langle \mathbf{x}'_1 | \mathbf{r}_{j_1}; g \rangle \sum_{j_2} \langle \mathbf{x}'_2 | \mathbf{r}_{j_2}; g \rangle \dots \sum_{j_\nu} \langle \mathbf{x}'_\nu | \mathbf{r}_{j_\nu}; g \rangle. \quad (2) \end{aligned}$$

The tensor products of $\langle \mathbf{x} | \rho \rangle$ describes the structure of the environment ($\nu = 1$ provides a full description at this level, but $\nu > 1$ will become necessary when symmetrizing the representation), while the Gaussian centered on the i -atoms identify the atom tuple for which $y_{i_1 i_2 \dots}$ is to be predicted. Figure 2(a) shows an example of atom-centered Gaussians and the total atom density for a 1D point cloud.

B. Translational symmetry

Averaging Eq. (2) over the translation group leads to a rather daunting expression: the convolution of $(N+\nu)$ Gaussian densities generates a product of $(N+\nu)(N+\nu-1)/2$ Gaussians relative to differences of the arguments of pairs of the densities (to be precise, with a variance that is increased by a factor of $(N+\nu)$ relative to the initial Gaussians),

$$\int d\hat{t} \langle \mathbf{x}_1; \mathbf{x}_2; \dots; \mathbf{x}_n; \mathbf{x}'_1; \mathbf{x}'_2; \dots; \mathbf{x}'_\nu | \hat{t} | \rho_{i_1 i_2 \dots i_N}^{\otimes \nu} \rangle \equiv \\ \sum_{j_1 j_2 \dots} \prod_{\substack{\alpha \in \{i_1 \dots j_1 \dots\} \\ \beta \in \{i_1 \dots j_1 \dots\}, \beta > \alpha}} \langle \mathbf{x}_\beta - \mathbf{x}_\alpha | \mathbf{r}_\beta - \mathbf{r}_\alpha; g \rangle, \quad (3)$$

where it is implied that $\mathbf{x}_{i_\alpha} \equiv \mathbf{x}_\alpha$ and $\mathbf{x}_{j_\alpha} \equiv \mathbf{x}'_\alpha$. Even though the result contains a large number of Gaussian factors, it only functionally depends on $(N+\nu-1)$ differences between the feature indices, $(\mathbf{x}_\beta - \mathbf{x}_\alpha)$ (see Fig. 2(b) for the simplest case where only the atom density $\langle \mathbf{x} | \rho \rangle$ is symmetrized over translations). We can pick the $i \equiv i_1$ atom as reference, define $\tilde{\mathbf{x}}_i = \mathbf{x}_i - \mathbf{x}_1$ and write

$$\begin{aligned} \langle \tilde{\mathbf{x}}_2; \dots; \tilde{\mathbf{x}}_n; \tilde{\mathbf{x}}'_1; \tilde{\mathbf{x}}'_2; \dots; \tilde{\mathbf{x}}'_\nu | \langle \rho_{ii_2 \dots i_N}^{\otimes \nu} \rangle_i \rangle \equiv \\ \prod_{\beta \in \{i_2 \dots i_N\}} \langle \tilde{\mathbf{x}}_\beta | \mathbf{r}_{\beta i}; g \rangle \sum_{j_1 \dots j_\nu} \prod_{\beta \in \{j_1 \dots j_\nu\}} \langle \tilde{\mathbf{x}}'_\beta | \mathbf{r}_{\beta i}; g \rangle \\ \times \prod_{\substack{\alpha \in \{i_2 \dots j_1 \dots\} \\ \beta \in \{i_2 \dots j_1 \dots\}, \beta > \alpha}} \langle \tilde{\mathbf{x}}_\beta - \tilde{\mathbf{x}}_\alpha | \mathbf{r}_{\beta i} - \mathbf{r}_{\alpha i}; g \rangle. \quad (4) \end{aligned}$$

The product on the third line contains largely redundant information (as it couples distance vectors that are already in the argument of Gaussians centered on the selected i atom), and is computationally problematic, as it couples the densities associated with different j indices preventing the application of the density trick that can be used to evaluate these features efficiently.³⁹ Thus, we just drop it altogether, reorder the indices, and define the atom-centered, translation-

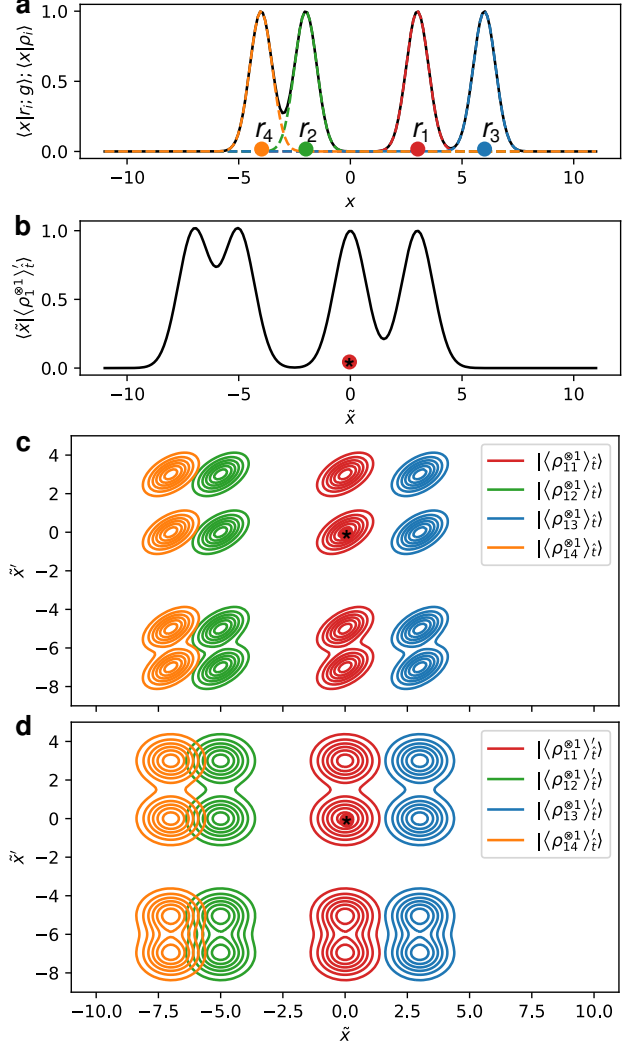


Figure 2: (a) A 1D group point cloud, represented together with the density contributions and the total atom density $\langle \mathbf{x} | \rho \rangle$. (b) The translationally-symmetrized density $\langle \mathbf{x} | \rho_i \rangle$ centered on the atom $i = 1$. (c) Translationally-symmetrized pair features $\langle \tilde{\mathbf{x}}; \tilde{\mathbf{x}}' | \langle \rho_{ii'}^{\otimes 1} \rangle_{\hat{t}} \rangle$, for $i = 1$, and with different i' represented with different colors. (d) As in (c), for the simplified form in Eq. (5).

invariant, permutation-equivariant features as

$$\begin{aligned} \langle \mathbf{x}_2; \dots; \mathbf{x}_n; \mathbf{x}'_1; \mathbf{x}'_2; \dots; \mathbf{x}'_\nu | \langle \rho_{ii_2 \dots i_N}^{\otimes \nu} \rangle'_{\hat{t}} \rangle \equiv \\ \prod_{\alpha=2}^N \langle \mathbf{x}_\alpha | \mathbf{r}_{i_\alpha i}; g \rangle \prod_{\beta=1}^\nu \langle \mathbf{x}'_\beta | \rho_i \rangle \quad (5) \end{aligned}$$

where we introduced the i -centered density $|A; \rho_i\rangle \equiv \sum_{j \in A} |\mathbf{r}_{ji}; g\rangle$. Figure 2(c-d) demonstrates, in a simple case, how Eq. (4) and (5) contain similar amounts of structural information.

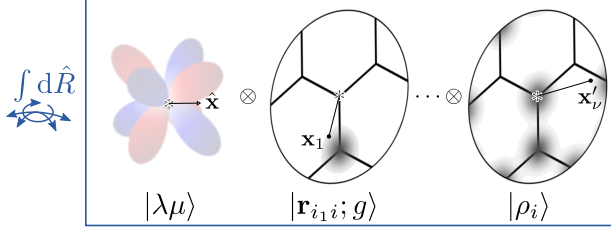


Figure 3: A schematic representation of the construction of $O(3)$ equivariant pair features, as the symmetry average of a tensor product of pair densities, a neighbor density and a set of spherical harmonics.

C. Rotational symmetry

Having selected one reference i -atom makes it simple to relate Eq. (5) to the $O(3)$ equivariant features that can be obtained by symmetrizing the ν -point neighbor density correlations¹³. For $N = 1$, this symmetry average amounts to

$$|\overline{\rho_i^{\otimes \nu}; \sigma; \lambda\mu}\rangle \equiv \int_{O(3)} d\hat{R} \prod_{\beta=1}^{\nu} \hat{R} |\rho_i\rangle \otimes \hat{R} |\sigma\rangle \otimes \hat{R} |\lambda\mu\rangle \quad (6)$$

where we use $d\hat{R}$ to indicate averaging over proper and improper (without and with inversion) rotations, we use a compact notation that does not indicate explicitly the basis, and $|\sigma; \lambda\mu\rangle$ tracks the transformation behavior with respect to the symmetry operation.⁴⁰ Including also the Gaussians that tag further centers is formally analogous:

$$|\overline{\rho_{i_2 \dots i_N}^{\otimes \nu}; \sigma; \lambda\mu}\rangle \equiv \int_{O(3)} d\hat{R} \prod_{\alpha=2}^N \hat{R} |\mathbf{r}_{i_\alpha i}; g\rangle \prod_{\beta=1}^{\nu} \hat{R} |\rho_i\rangle \otimes \hat{R} |\sigma\rangle \otimes \hat{R} |\lambda\mu\rangle, \quad (7)$$

providing the general, abstract expression for the N -centers, ν -neighbors symmetrized density correlation equivariants, that is represented schematically in Fig. 3. With these definitions, one recognizes a connection between different N -center features,

$$\sum_{i_N} |\overline{\rho_{i_2 \dots i_N}^{\otimes \nu}; \sigma; \lambda\mu}\rangle = |\overline{\rho_{i_2 \dots i_{N-1}}^{\otimes \nu+1}; \sigma; \lambda\mu}\rangle. \quad (8)$$

By summing over all of the centers in a structure, one eliminates the dependence of N -center features on one of the i indices, and convert them into a $(N-1)$ -center representation of higher body order. In other terms, one could take N -center, $\nu = 0$ equivariants as the starting point of the construction, and make them invariant with respect to atom index permutations by summing over all the i indices – effectively building permutation-invariant representations by summing over ν -center clusters rather than by symmetrized products of $|\rho_i\rangle$.³⁹

To compute these descriptors in practice, it suffices to expand the neighbor densities in radial functions $\langle x|nl\rangle$ and spherical harmonics $\langle \mathbf{x}|lm\rangle$

$$\langle nlm|\mathbf{r}_{ji}; g\rangle \equiv \int d\mathbf{x} \langle nl|x\rangle \langle lm|\hat{\mathbf{x}}\rangle \langle \mathbf{x}|\mathbf{r}_{ji}; g\rangle, \quad (9)$$

and apply expressions that are entirely analogous to those for the $(N+\nu)$ -neighbors density correlation features.^{13,39,40} Note that in practical implementations, including the one we use here, one usually adopts real spherical harmonics, which requires using a consistent definition of the angular momentum sum rules.⁴¹ The expressions we write in the text assume real-valued coefficients. Considering invariant pair features $|\overline{\rho_{ii'}^{\otimes \nu}}\rangle$ one gets the two-centers, zero-neighbors term

$$\langle n|\overline{\rho_{ii'}^{\otimes 0}}\rangle \equiv \langle n00|\mathbf{r}_{ii'}; g\rangle, \quad (10)$$

the two-centers, one-neighbor features

$$\langle n_1 n_2 l|\overline{\rho_{ii'}^{\otimes 1}}\rangle \equiv \sum_m \frac{1}{\sqrt{2l+1}} \langle n_1 lm|\mathbf{r}_{ii'}; g\rangle \langle n_2 lm|\rho_i\rangle, \quad (11)$$

or the 3-centers, zero-neighbor features

$$\langle n_1 n_2 l|\overline{\rho_{ii_2 i_3}^{\otimes 0}}\rangle \equiv \sum_m \frac{1}{\sqrt{2l+1}} \langle n_1 lm|\mathbf{r}_{i_2 i}; g\rangle \langle n_2 lm|\mathbf{r}_{i_3 i}; g\rangle, \quad (12)$$

and so on and so forth.

Similar constructions can be applied to other atom-centered frameworks, such as moment tensor potentials⁸, or the atomic cluster expansion¹⁴. Given the fundamental equivalence with the density-correlation frameworks, it may also be possible to extend atom-centered symmetry functions⁴² or the FCHL features¹² in the same direction. Higher-body order equivariant features can be easily obtained within the N -body iterative contraction (NICE) framework⁴⁰, applying an iteration of the form

$$\begin{aligned} & \langle \dots; nlk|\overline{\rho_{i \dots i_N}^{\otimes (\nu+1)}; \sigma; \lambda\mu}\rangle \\ & \propto \sum_{mq} \langle lm; kq|\lambda\mu\rangle \langle nlm|\rho_i\rangle \\ & \times \langle \dots|\overline{\rho_{i \dots i_N}^{\otimes \nu}; (\sigma(-1)^{l+k+\lambda}); kq}\rangle \end{aligned} \quad (13)$$

to increase the order of the neighbor-density description, and

$$\begin{aligned} & \langle \dots; nlk|\overline{\rho_{i \dots i_{N+1}}^{\otimes \nu}; \sigma; \lambda\mu}\rangle \\ & \propto \sum_{mq} \langle lm; kq|\lambda\mu\rangle \langle nlm|\mathbf{r}_{i_{N+1} i}; g\rangle \\ & \times \langle \dots|\overline{\rho_{i \dots i_N}^{\otimes \nu}; (\sigma(-1)^{l+k+\lambda}); kq}\rangle \end{aligned} \quad (14)$$

to include an additional center to the feature.

D. Index permutation symmetry

Expressing the translationally-symmetrized N -center features in a compact, non-redundant basis,

and selecting one i -atom as the origin for their construction (that is, discarding the cumbersome term in (4)) simplifies greatly their evaluation and manipulation. However, it obscures the symmetry of the features with respect to permutations of the N -center indices, which can be problematic when one wants to learn e.g. a 2-center quantity that is symmetric with respect to a swap of the i indices. To address this further symmetry, we define permutation-symmetrized N -center features

$$|\rho_{i_1 i_2 \dots i_N}^{\otimes \nu}; \pi\rangle \equiv \sum_{\mathbf{p} \in \text{perm}(N)} \text{sign}_{\pi}(\mathbf{p}) |\rho_{i_{p_1} i_{p_2} \dots i_{p_N}}^{\otimes \nu}\rangle. \quad (15)$$

For example, the symmetric and antisymmetric pair features can be easily obtained as

$$|\rho_{ii'}^{\otimes \nu}; \alpha; \pm\rangle = |\rho_{ii'}^{\otimes \nu}; \alpha\rangle \pm |\rho_{i'i}^{\otimes \nu}; \alpha\rangle, \quad (16)$$

where α stands for any additional symmetry index, such as parity σ or rotational indices $\lambda\mu$.

III. LEARNING ATOMIC-ORBITAL MATRICES

As a practical application of the N -center representations, let us consider the case of modeling the matrix elements of the electronic Hamiltonian, written in a basis of atom-centered orbitals

$$\langle \hat{H}; a_i \tilde{n} \tilde{l} \tilde{m}; a_{i'} \tilde{n}' \tilde{l}' \tilde{m}' | A_{ii'} \rangle \equiv \langle i \tilde{n} \tilde{l} \tilde{m} | \hat{H} | i' \tilde{n}' \tilde{l}' \tilde{m}' \rangle. \quad (17)$$

We use a tilde decoration to distinguish the orbital indices from the indices used to enumerate pair features, and we recast the usual matrix-element notation from quantum mechanics into one that is more suitable to enumerate the learning targets in a ML exercise. The Hamiltonian is just one of the many matrices describing pair terms in electronic-structure theory, and other entities that could be manipulated in the same way include the density matrix and the orbital overlap. The bra on the left-hand side enumerates the entries in the Hamiltonian matrix, which can be broken down into blocks, each of which is associated with a distinct model that should be separately trained to be able to reconstruct the full matrix. For each *type* of blocks (atomic species, radial channels, ...) we are going to build models that take as inputs the features associated with a pair $A_{ii'}$ and predict the corresponding section of the Hamiltonian. To give a concrete example of the architecture we are considering, a linear model to predict the matrix element between the $2s$ and $1s$ orbitals on a O and H atom can be written as

$$\langle \hat{H}; O200; H100 | A_{ii'} \rangle \approx \sum_q \langle \hat{H}; O2s; H1s | q \rangle \langle q | A_{ii'}; 00 \rangle, \quad (18)$$

where q indicates the discretization of the feature vector. The regression weights are specific to the type of the block ($O2s; H1s$), while the features describe the two selected atoms and their environment, and have

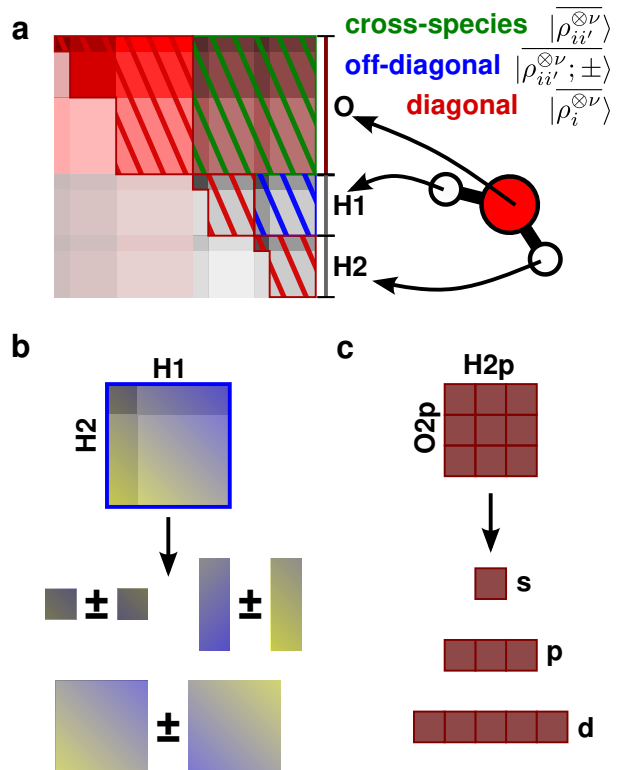


Figure 4: (a) A schematic representation of the different types of blocks that compose the Hamiltonian for a water molecule. (b) Blocks involving different atoms of the same species must be transformed into the index-permutation equivariant forms. (c) The $O(3)$ equivariance of different angular momentum blocks can be simplified by converting them into a coupled basis, separating their irreducible components.

the appropriate equivariance ($\lambda = 0$) for the orbitals under consideration. While it would be possible, and probably beneficial, to adapt the hyperparameters of the features depending on the orbital type, we will use the same set of features for all blocks with equivalent symmetry, e.g. we use exactly the same $\langle q | A_{ii'}; 00 \rangle$ when predicting the ($O1s; H1s$) block type.

A. Permutation equivariance

The entries in the Hamiltonian are not fully symmetric, and it is advisable to convert them in an irreducible form. First, we need to consider the symmetry with respect to the swaps of atom and orbital labels. The simultaneous swap of atom and orbital corresponds to the Hermitian symmetry of the Hamiltonian:

$$\langle \hat{H}; a_i \tilde{n} \tilde{l} \tilde{m}; a_{i'} \tilde{n}' \tilde{l}' \tilde{m}' | A_{ii'} \rangle = \langle \hat{H}; a_{i'} \tilde{n}' \tilde{l}' \tilde{m}'; a_i \tilde{n} \tilde{l} \tilde{m}; | A_{i'i} \rangle^*. \quad (19)$$

In fact, we will work with Hamiltonians written using real-valued spherical harmonics, and so the matrix is

real and symmetric. This means that only half of the Hamiltonian needs to be predicted. To obtain perfect equivariance with respect to the sorting of atomic indices, one should proceed with care in handling blocks associated with different types of atoms.

Cross-element terms. Consider first the case of matrix elements between atoms of different species. We can always choose to pick the atoms in a prescribed order, e.g. consider the heavier element as the first in the pair. Still, we need a separate model for each combination of orbitals on the two centers: there is no symmetry relationship between $(a\tilde{n}\tilde{l}; a'\tilde{n}'\tilde{l}')$ and $(a\tilde{n}'\tilde{l}'; a'\tilde{n}\tilde{l})$, even if one uses the same radial basis for both elements, because e.g. the matrix element for a $1s$ orbital centered on O and a $2s$ orbital centered on H is different from the matrix element for a $2s$ orbital centered on O and a $1s$ orbital centered on H. The element types that define the block type also induce a natural ordering of the pair – that is, one can choose consistently the order of the indices (i, i') in the pair features. Thus, there is no need to use features with a specified particle-exchange symmetry – one could use either $|\rho_{ii'}^{\otimes\nu}\rangle$, $|\rho_{i'i}^{\otimes\nu}\rangle$. To incorporate the maximum amount of information, and to have a scheme that is independent on an arbitrary choice of ordering, we concatenate the two asymmetric pair features $|\rho_{ii'}^{\otimes\nu}\rangle \oplus |\rho_{i'i}^{\otimes\nu}\rangle$.

Same-element, off-diagonal terms. These terms require particular attention. Contrary to the previous case, one cannot choose a priori the order of the atoms in the pair, because they are indistinguishable. The matrix elements, however, are not symmetric with respect to the swap of atom indices (i, i') . To give a concrete example $\langle \hat{H}; O100; O200 | A_{37} \rangle$ has no prescribed relationship to $\langle \hat{H}; O100; O200 | A_{73} \rangle$, because the environment of the O atom at \mathbf{r}_7 might be completely different from that at \mathbf{r}_3 . When given a new structure to predict, however, we only know there are two O centers and we want to predict a matrix element for $(O100; O200)$, so the weights would be the same for A_{37} and A_{73} . Even though the asymmetric $|\rho_{37}^{\otimes\nu}\rangle$ and $|\rho_{73}^{\otimes\nu}\rangle$ differ, there is no reason they should – when combined with the *same set of weights* – give meaningful predictions for the two sets of elements of \hat{H} . In other terms, given that we cannot fix the order of the two centers to match the orbital blocks associated with them, we cannot build a model that depends on the ordering of the atoms of each species.

To address this issue, we need to modify the target so that it is equivariant with respect to a swap of the center indices. This can be achieved by building symmetric and antisymmetric combinations of the entries

$$\begin{aligned} \langle \hat{H}; a_i \tilde{n} \tilde{l} \tilde{m}; a_i \tilde{n}' \tilde{l}' \tilde{m}'; \pm | A_{ii'} \rangle &\equiv \\ \langle \hat{H}; a_i \tilde{n} \tilde{l} \tilde{m}; a_i \tilde{n}' \tilde{l}' \tilde{m}' | A_{ii'} \rangle &\pm \langle \hat{H}; a_i \tilde{n} \tilde{l} \tilde{m}; a_i \tilde{n}' \tilde{l}' \tilde{m}' | A_{i'i} \rangle. \end{aligned} \quad (20)$$

Given that these combinations transform in a precise way under an exchange of the particle indices, they

can be suitably learned with the symmetric and antisymmetric pair features (16), $|\rho_{ii'}^{\otimes\nu}; \pm\rangle$. Furthermore, one can exploit Hermitian symmetry, and learn only models for lexicographically-ordered $(\tilde{n}\tilde{l}, \tilde{n}'\tilde{l}')$ terms, i.e. for $\tilde{n}' \geq \tilde{n}$, and (when $\tilde{n}' = \tilde{n}$) $\tilde{l}' \geq \tilde{l}$. Terms that correspond to $(\tilde{n}', \tilde{l}') = (\tilde{n}, \tilde{l})$ are special, because swapping the atom indices corresponds to taking the transpose of the block. As a consequence, due to the Hermitian property of the Hamiltonian, some of the symmetrized terms are bound to be zero (see the SI).

Diagonal terms. Terms that correspond to on-site blocks, $i = i'$ should not be considered pair terms at all, and are best learned using one-center features $|\rho_i^{\otimes\nu}\rangle$. Similar to the same-species case, thanks to the Hermitian symmetry, we only need to build models for the lexicographically ordered orbital pairs.

B. $O(3)$ equivariance

The Hamiltonian block $\langle \hat{H}; \tilde{n} \tilde{l} \tilde{m}; \tilde{n}' \tilde{l}' \tilde{m}' | A_{ii'} \rangle$ transforms as a product of (real) spherical harmonics,⁴³ $|\tilde{l}\tilde{m}\rangle \otimes |\tilde{l}'\tilde{m}'\rangle$. We omit the indication of the nature of the elements, and the possible symmetrization with respect to atom indices permutation, because the same arguments apply to each type of blocks discussed in the previous paragraph. We can use well-known relationships between products and sums of spherical harmonics to convert the matrix elements into irreducible representations of $SO(3)$:

$$\begin{aligned} \langle \hat{H}; \tilde{n} \tilde{l}; \tilde{n}' \tilde{l}'; \lambda\mu | A_{ii'} \rangle &= \sum_{\tilde{m}\tilde{m}'} \langle \hat{H}; \tilde{n} \tilde{l} \tilde{m}; \tilde{n}' \tilde{l}' \tilde{m}' | A_{ii'} \rangle \\ &\times \langle \tilde{l}\tilde{m}; \tilde{l}'\tilde{m}' | \lambda\mu \rangle \end{aligned} \quad (21)$$

and back

$$\begin{aligned} \langle \hat{H}; \tilde{n} \tilde{l} \tilde{m}; \tilde{n}' \tilde{l}' \tilde{m}' | A_{ii'} \rangle &= \sum_{\lambda\mu} \langle \hat{H}; \tilde{n} \tilde{l}; \tilde{n}' \tilde{l}'; \lambda\mu | A_{ii'} \rangle \\ &\times \langle \tilde{l}\tilde{m}; \tilde{l}'\tilde{m}' | \lambda\mu \rangle. \end{aligned} \quad (22)$$

This is preferable to building symmetry-adapted models for the uncoupled basis (which would be possible with minor modifications of the equivariant construction) because we can re-use the same framework that is routinely applied to the learning of tensorial properties²⁰ – i.e. the symmetry-adapted equivariant features, extended here to multi-center $|\rho_{i\dots i_N}^{\otimes\nu}; \lambda\mu\rangle$ – and because the learning of large blocks of geometrically covariant terms is broken down into smaller terms that correspond to irreducible representations of $O(3)$. For the off-diagonal, same species blocks, the coupled-basis form of the Hamiltonian matrix elements can then be symmetrized with respect to atom-index exchange, yielding quantities of the form $\langle \hat{H}; \tilde{n} \tilde{l}; \tilde{n}' \tilde{l}'; \lambda\mu; \pm | A_{ii'} \rangle$ that can be learned with the corresponding symmetric and antisymmetric pair features.

A subtle point to consider is that the coupled angular basis elements (21) transform as Y_λ^μ under

$SO(3)$ (proper) rotations, but behave differently under $O(3)$ (improper) rotations. While spherical harmonics transform under inversion as polar tensors $\hat{i}|\lambda\mu\rangle = (-1)^\lambda|\lambda\mu\rangle$, some of the coupled basis terms transform as pseudotensors, $\hat{i}|\lambda\mu\rangle = (-1)^{\lambda+1}|\lambda\mu\rangle$. For instance, consider the case of $(\tilde{l} = 1, \tilde{l}' = 1)$. The product $|1\tilde{m}\rangle \otimes |1\tilde{m}'\rangle$ is even under inversion (because each term is odd); and so the $\lambda = 1$ coupled terms $|\tilde{l} = 1; \tilde{l}' = 1; \lambda = 1 \mu\rangle$ must also be even - and thus behave as a pseudovector. In general, the parity of a block of the Hamiltonian in the coupled form $\langle \hat{H}; \tilde{n}\tilde{l}; \tilde{n}'\tilde{l}'; \lambda\mu | A_{ii'} \rangle$ is $\sigma = (-1)^{\tilde{l}+\tilde{l}'+\lambda}$. Given that the NICE iterations (13)-(14) provide a natural strategy to track the parity of the equivariant features, it is possible to exploit this additional symmetry, that has been shown to increase the transferability of the resulting models in the context of λ -SOAP-based symmetry-adapted Gaussian process regression⁴⁴. We conclude noting that for the matrix elements corresponding to the same element and orbital index, parity and index exchange symmetry are linked, resulting in some blocks of the coupled-momentum Hamiltonian being identically zero.

C. Symmetry-adapted regression

Armed with a set of symmetry-adapted features, and with a transformation of the Hamiltonian into irreducible symmetry blocks, we can proceed to construct regression models. Given the emphasis we give to the construction of well-principled features, we restrict ourselves to simple models, but it would be relatively simple to build an $O(3)$ equivariant neural network^{13,21}, using the equivariant features as inputs.

For each block $Q = (a\tilde{n}\tilde{l}; a'\tilde{n}'\tilde{l}'; \eta)$ (where η indicates the equivariance and symmetry with respect to index exchange, if relevant), and rotationally-equivariant component λ , a linear regression model reads

$$\langle \hat{H}; Q; \lambda\mu | A_{ii'} \rangle \approx \sum_q \langle \hat{H}; Q; \lambda; q \rangle \langle q | A_{ii'}; \text{sym}(Q); \lambda\mu \rangle, \quad (23)$$

where we indicate with “ $\text{sym}(Q)$ ” that the features should have symmetries matching those of the Hamiltonian block. Even though it may be advantageous to separately tune the hyperparameters of the representation depending on the type of block, here we use the same features to regress all blocks having the same symmetry. The symmetry-adapted regression weights $w_q^{(Q,\lambda)} = \langle \hat{H}; Q; \lambda; q \rangle$ can be determined computing a symmetrized covariance matrix

$$C_{qq'}^{(Q,\lambda)} = \sum_{ii' \in Q, \mu} \langle A_{ii'}; \text{sym}(Q); \lambda\mu | q \rangle \langle q' | A_{ii'}; \text{sym}(Q); \lambda\mu \rangle \quad (24)$$

and feature-weighted targets

$$z_q^{(Q,\lambda)} = \sum_{ii' \in Q, \mu} \langle \hat{H}; Q; \lambda\mu | A_{ii'} \rangle \langle A_{ii'}; \text{sym}(Q); \lambda\mu | q \rangle, \quad (25)$$

and then evaluating a ridge-regression expression

$$\mathbf{w}^{(Q,\lambda)} = (\mathbf{C}^{(Q,\lambda)} + \sigma^2 \mathbf{1})^{-1} \mathbf{z}^{(Q,\lambda)}, \quad (26)$$

where σ is a regularization parameter, that can be optimized by cross-validation.

We also test a kernel-based symmetry-adapted Gaussian-process regression (SA-GPR) model. We compute symmetry-adapted kernels that generalize to the multi-center case the λ -SOAP kernel of Ref. 20

$$k_{\mu\mu'}^{(Q,\lambda)}(A_{ii_2}, A'_{i'i_2}) = \sum_q \langle A_{ii_2}; \text{sym}(Q); \lambda\mu | q \rangle \langle q | A'_{i'i_2}; \text{sym}(Q); \lambda\mu' \rangle \quad (27)$$

and then formulate a SA-GPR ansatz

$$\langle \hat{H}; Q; \lambda\mu | A_{ii'} \rangle \approx \sum_{M\mu'} b_{M\mu'}^{(Q,\lambda)} k_{\mu\mu'}^{(Q,\lambda)}(A_{ii'}, M), \quad (28)$$

where M indicates a collection of “active” points selected among the atomic environments (or pairs) in the training set. In the projected-process approximation, one can then compute the kernel regression weights by

$$\mathbf{b}^{(Q,\lambda)} = (\mathbf{K}_{NM}^T \mathbf{K}_{NM} + \sigma^2 \mathbf{K}_{MM})^{-1} \mathbf{K}_{NM}^T \quad (29)$$

where \mathbf{K}_{MM} and \mathbf{K}_{NM} indicate respectively the matrices collecting the kernels between the active-set clusters and those between training and active-set clusters⁴. The cluster index and the angular momentum index μ are merged in a single index. An important difference with previous applications of SA-GPR is that one should be careful when using non-linear kernels built by combining an invariant $\lambda = 0$ and a $\lambda > 0$ kernel^{13,25}. In fact, some of the invariant features may be zero because of molecular symmetries, while some of the corresponding $\lambda > 0$ features are not. This leads to scenarios in which k_{00}^0 , but not $k_{\mu\mu'}^\lambda$, vanishes. Thus, we define non-linear kernels as products of the equivariant linear kernel(27) with a polynomial in the invariant kernel,

$$k_{\mu\mu'}^{(\zeta, Q, \lambda)}(A, A') = k_{\mu\mu'}^{(Q, \lambda)}(A, A') \sum_{p=0}^{p_{\max}} \zeta_p k^{(Q, 0)}(A, A')^p. \quad (30)$$

The $p = 0$ term ensures a non-zero values also in the few cases in which the scalar kernel vanishes because of symmetry.

D. Regression of non-orthogonal Hamiltonians

The atomic orbital basis is non-orthogonal, which means that – in order to obtain the single-particle

wavefunction coefficients matrix \mathbf{U} and eigenvalues ϵ from the Hamiltonian matrix \mathbf{U} – one needs to solve a generalized eigenvalue equation,

$$\mathbf{H}\mathbf{U} = \mathbf{S}\mathbf{U} \text{ diag } \epsilon, \quad (31)$$

where \mathbf{S} is the overlap matrix associated with the molecule. We can avoid learning separately a model for the overlap matrix, and get predictions that can directly be diagonalized to obtain the same single-particle energy levels as from Eq. (31), by first computing the Löwdin-orthogonalized Hamiltonian,

$$\bar{\mathbf{H}} = \mathbf{S}^{-1/2} \mathbf{H} \mathbf{S}^{-1/2}, \quad (32)$$

and then using it as a regression target. The orthogonal Hamiltonian $\bar{\mathbf{H}}$ obeys exactly the same symmetries as \mathbf{H} . Even though, as we shall see, it is more difficult to learn, it leads to more comparably-accurate predictions for the eigenvalues. Unless otherwise specified, in all numerical benchmarks we will build models for the Löwdin-orthogonalized Hamiltonian matrix.

IV. CONTINUOUS SYMMETRIES AND MOLECULAR SYMMETRIES

By incorporating all permutation, rotation and inversion symmetries, a Hamiltonian predicted based on these features is guaranteed to be equivariant to all point-group operations that may be present for a symmetric molecular geometry. This is a consequence of the fact that point groups are a subgroup of the combination of $O(3)$ operations and permutations,^{45–47} and would also generalize to space groups symmetries, thanks to the fact that N -center representations are also translationally invariant. As a consequence, the eigenfunctions of \hat{H} must transform according to irreducible representations of the point group, and those that transform into each other under point group operations must be degenerate.

To explore this observation, consider benzene at its equilibrium geometry. Atomic orbitals centred on each of the atoms generate a reducible representation Γ of D_{6h} , the point group that the geometry corresponds to. This reducible representation can be decomposed uniquely into irreducible components,

$$\Gamma = a_1\Gamma_1 \oplus a_2\Gamma_2 \oplus \cdots \oplus a_k\Gamma_k, \quad (33)$$

where Γ_l are irreducible representations of D_{6h} . Simply by recognising that the Hamiltonian satisfies the point group symmetries (i.e., commutes with all the symmetry elements), we can conclude that the molecular orbitals obtained from this basis must transform according to the irreducible representations appearing on the right-hand side of the decomposition written above. This has an immediate consequence on the structure of the energy levels: if there are k l -dimensional irreducible representations in the decomposition, there must be k energy levels which are l -fold degenerate. To further refine the energy

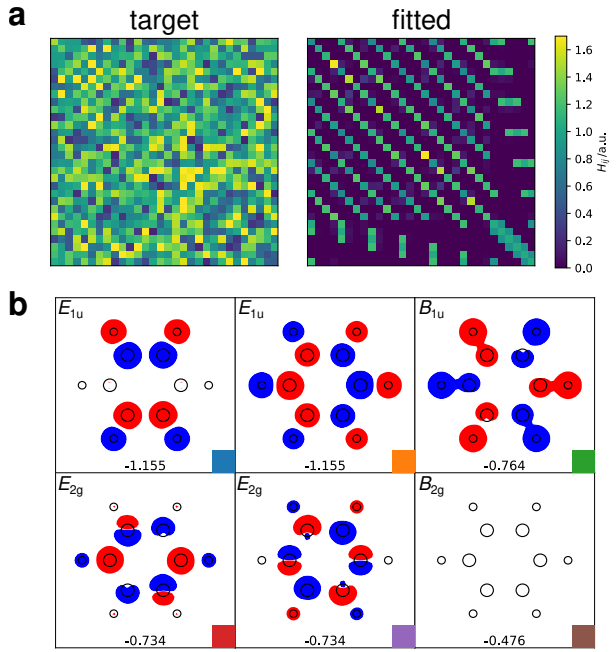


Figure 5: (a) A minimal-basis Hamiltonian for benzene. Left: filled with random numbers, right: predicted by a symmetry-adapted model after learning on the random target. (b) The first six eigenstates of the predicted Hamiltonians. This is just a cartoon representation built from the isocontours of a fictional wavefunction built from atomic orbitals that combine a single Gaussian function centered on the atoms with the appropriate real spherical harmonics, evaluated in the plane of the molecule. The sixth state has a nodal surface in the plane.

level diagram, we can estimate the coupling through the Hamiltonian of symmetry-adapted linear combinations of atomic orbitals. The coupling between symmetry-adapted linear combinations belonging to different irreducible representation is strictly zero. The magnitude of the other couplings cannot be determined based on symmetry, but can be estimated from physical principles.

The procedure just described is familiar to all chemists as molecular orbital theory, a cornerstone of modern chemistry, which can be remarkably successful in describing the bonding and stability of molecules. Exploiting point-group symmetry is an indispensable part of the procedure, and the small number of simple rules that are commonly used to refine an energy level diagram are independent of the constraints imposed by symmetry. In other words, modifying the rules cannot affect the features of the energy level structure that are constrained on symmetry grounds. Since the Hamiltonians generated by our model are guaranteed to satisfy point group symmetries, the model is forced to operate in much the same way. The model extracts from training data the information that cannot be determined based on symmetry alone, and it can-

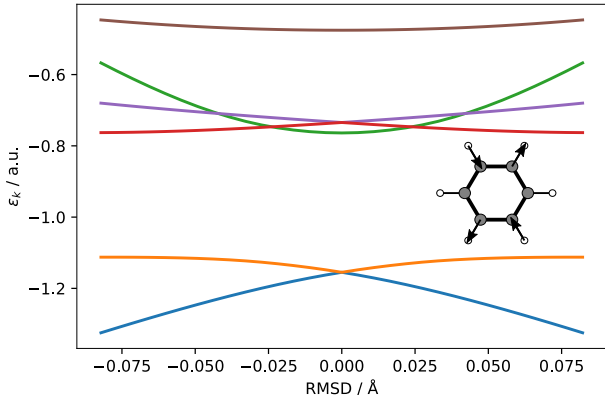


Figure 6: An example of the changes in energy levels associated with a E_{2g} symmetric deformation of the benzene molecule, computed from a minimal-basis Hamiltonian. The matrix elements are predicted from a model trained on a single random-valued matrix.

not help but predict the correct energy level structure and molecular orbital symmetries.

As a numerical example, we build a 30×30 matrix filled with uniform random numbers between 0 and 1, symmetrized by adding its own transpose, and we interpret it as the single-electron Hamiltonian of benzene at the equilibrium geometry in a minimal valence basis (C_{2s} , C_{2p} , H_{1s}). We train our model on this single configuration. The model cannot reproduce the random Hamiltonian because it is incompatible with the molecular symmetry. Instead, it learns a matrix which reveals the symmetry of the system (Figure 5a). Furthermore, the molecular orbitals of the predicted Hamiltonian (which we compute assuming the functions in the minimal basis are orthogonal) transform according to irreducible representations of D_{6h} , and the degeneracy of the energy levels is thus correct. The representation generated by the minimal basis decomposes into irreducible components as follows,

$$\Gamma = 2A_{1g} \oplus A_{2u} \oplus 2B_{1u} \oplus B_{2g} \oplus E_{1g} \oplus 2E_{1u} \oplus 2E_{2g} \oplus E_{2u}. \quad (34)$$

The predicted Hamiltonian thus exhibits at least six doubly-degenerate energy levels (corresponding to molecular orbitals with E symmetry). Figure 5b shows the six lowest-lying molecular orbitals, labelled with irreducible representations, four of which are doubly degenerate. Even though the model is trained with nonsensical data, the appearance of the predicted molecular orbitals and their degeneracies are qualitatively correct. Quantitative accuracy could be obtained by exposing the model to physically-meaningful training data. Note that exactly the same model, exposed to no more training data would predict a Hamiltonian of Buckminsterfullerene, for example, satisfying all of the 120 point group symmetries – although it might also fulfil additional symmetries, because D_{6h} is not a subgroup of I_h .

This numerical example demonstrates the well-known fact that symmetry considerations are often indispensable when solving problems in quantum mechanics. Any behaviour governed by point group symmetry must be replicated by our model. Consider for instance the breaking of degeneracy as the molecule distorts away from a high-symmetry geometry, as in the celebrated Jahn-Teller theorem.⁴⁸ Continuing with the numerical example, the symmetric squares of E_{1u} and E_{2g} are the same,

$$[E_{1u} \otimes E_{1u}] = A_{1g} \oplus E_{2g}. \quad (35)$$

Therefore, we expect the degeneracy of the E_{1u} and E_{2g} energy levels of our predicted Hamiltonian to be broken by distortions of the geometry along normal modes of E_{2g} symmetry. The variation of the degenerate levels along such a normal mode should vary to first order in the displacement. On the other hand, the B_{1g} and B_{1u} energy levels should not vary to first order in the displacement. This analysis is confirmed by the variation of the energy levels in Figure 6 and has a clear consequence on the way that incorporating symmetry facilitates learning: the symmetry of a geometry not only places constraints on the Hamiltonian at that geometry but also dictates how the Hamiltonian must change when the geometry is distorted. This imposes a subtle structure on the form on the Hamiltonian as a function of geometry that a symmetry-unaware model would have to learn through exposure to training data.

V. EXAMPLES AND BENCHMARKS

We now discuss results for a few examples of increasing complexity and diversity. Our main objective will be to demonstrate the advantages of using symmetry-adapted features, but we will also discuss the role of the model, and compute a few of the properties one may want to extract from the exercise of predicting an atomic Hamiltonian. We note also that existing schemes show wildly different performances depending on the basis set used, and the number of energy levels targeted by the model. Ref. 33 provides a thorough comparison, showing that errors for the same dataset and model vary by more than an order of magnitude depending on the range of the spectrum targeted. Here we concern ourselves only with the full Hamiltonian matrix, and compute the entire eigenspectrum, and so the comparison with existing models, that predict eigenvalues in a restricted energy range, can only be qualitative. We also do not attempt to optimize the hyperparameters of the descriptors (cutoff distance, Gaussian smearing, ...) – in part for simplicity, in part because we use the same features for all blocks, and we want to avoid optimizing them for a specific type of matrix elements. The only optimization we consider, for each block type and train set size, is that of the ridge regularization, which we perform by grid search and 3-fold cross validation.

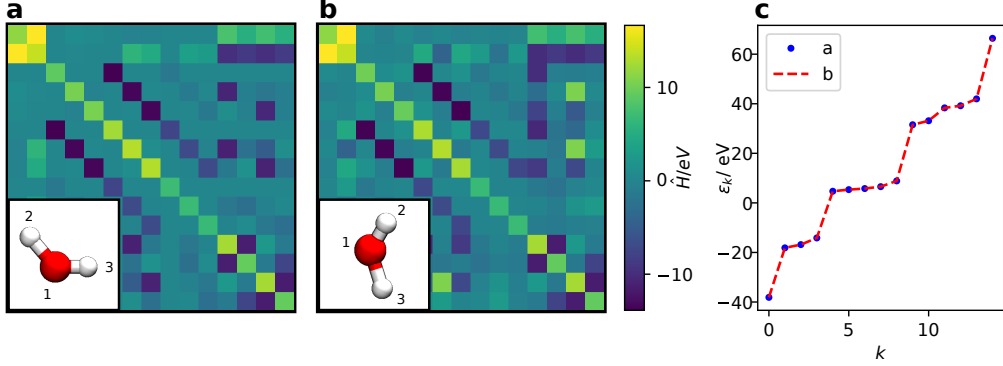


Figure 7: Equivariance of predictions under rotation of a distorted water molecule and permutation of its H atoms. The prediction in Fig b) is obtained by a model trained on the orthogonalized Fock matrix of a molecule in a). Even though the individual matrix elements are different, the eigenvalues are predicted to be exactly the same, within machine precision.

A. Datasets, computational details, and metrics

We used three different datasets: (1) a dataset of 1000 H_2O configurations that was originally introduced in Ref. 20 to demonstrate symmetry-adapted regression of tensors, that can be downloaded from a public data record⁴⁹; (2) the $\text{CH}_3\text{CH}_2\text{OH}$ trajectory used in Ref. 37, which we use together with the corresponding Hamiltonian matrices to provide a 1:1 comparison; (3) the subset of 6868 molecules from the QM7b dataset⁵⁰ that contains only CHNO atoms.

For datasets (1) and (3) we performed restricted Hartree Fock calculations using the quantum chemistry code, PySCF^{51,52} with the 6-31G basis for hydrogen and the Stuttgart effective core potential (ECP) and basis on all other atoms. A convergence threshold of $1e-10$ atomic units for both energies and gradients was set. The Hamiltonian and the overlap matrices obtained in the atomic-orbital basis were then transformed to the Löwdin orthogonalized basis as described in Section III D.

We define the mean square error associated with the overall prediction \hat{H} of the (orthogonal) Hamiltonian matrices over a given test set as

$$\text{MSE}_{\text{full}} = \frac{1}{N_{\text{test}}} \sum_{A \in \text{test}} \frac{1}{N_A} \times \sum_{iQ_i'Q'} |\langle \hat{H}; Q; Q' | A_{ii'} \rangle - \langle \tilde{H}; Q; Q' | A_{ii'} \rangle|^2, \quad (36)$$

where N_{test} is the number of structures in the test set and N_A indicates the size of the Hamiltonian matrix, i.e. the total number of atomic orbitals, and we use the notation of Eq. (17) to indicate summation over all the elements in the Hamiltonian matrix. We also compute errors for individual symmetry-adapted

blocks,

$$\text{MSE}_{Q\lambda} = \frac{1}{N_{\text{test}}} \sum_{A \in \text{test}} \frac{1}{N_A} \times \sum_{\mu, ii' \in Q} |\langle \hat{H}; Q; \lambda\mu | A_{ii'} \rangle - \langle \tilde{H}; Q; \lambda\mu | A_{ii'} \rangle|^2, \quad (37)$$

where we use the coupled-blocks notation (21) in which $Q \equiv (\tilde{n}\tilde{l}; \tilde{n}'\tilde{l}'; \pm)$. Eq. (37) is defined in such a way that summing over all blocks (making sure to account for the multiplicity of each block in the full Hamiltonian) yields the same value as the full MSE (36). We also compute errors for the eigenspectrum

$$\text{MSE}_\epsilon = \frac{1}{N_{\text{test}}} \sum_{A \in \text{test}} \frac{1}{N_A} \sum_k |\epsilon_k - \tilde{\epsilon}_k|^2 \quad (38)$$

where N_{test} is the number of structures in the test set and ϵ_k and $\tilde{\epsilon}_k$ are the sorted eigenvalues of the Hamiltonian and their predictions. We typically report root mean square errors (RMSE) that are simply the square roots of the definitions given above.

B. Water molecule

We begin showing results for the prediction of the valence Fock matrix of a dataset of 1000 distorted water molecules. Given that water is composed of only three atoms, $\nu = 2$ features provide a complete basis to regress the diagonal blocks, and $N = 2, \nu = 1$ features for the off-diagonal terms. We then limit ourselves to a linear regression scheme, using features built from neighbor density expansion coefficients with $r_{\text{cut}} = 4 \text{ \AA}$, $\sigma_a = 0.3 \text{ \AA}$, $n_{\text{max}} = 8$, $l_{\text{max}} = 6$. The radial basis was further optimized using the scheme of Ref. 41. Figure 7 demonstrates the equivariance of the model by training a linear model on the orthogonalized Fock matrix of a single distorted structure, and then making a prediction for another

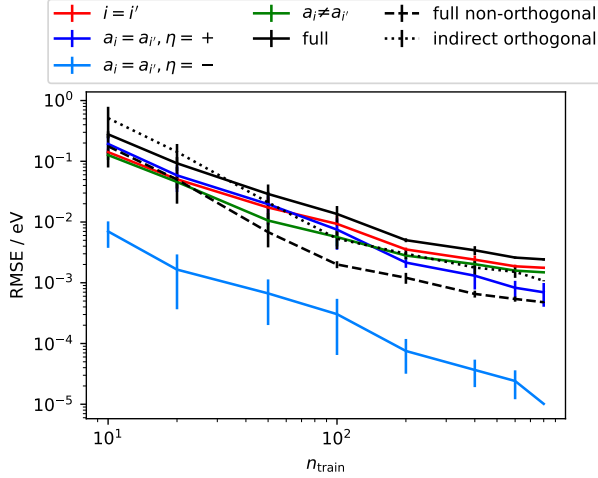


Figure 8: Learning curve for the matrix elements in different blocks of the Hamiltonian for a test set of 200 water molecules. Full lines correspond to linear ridge regression models trained on the Löwdin orthogonalized Hamiltonian matrices $\bar{\mathbf{H}}$, based on $(N = 2, \nu = 1)$ features. Errors for predicting the full non-orthogonalized matrix \mathbf{H} matrix are shown with dashed lines, while dotted lines indicates the error for computing $\bar{\mathbf{H}}$ by orthogonalizing the prediction for \mathbf{H} .

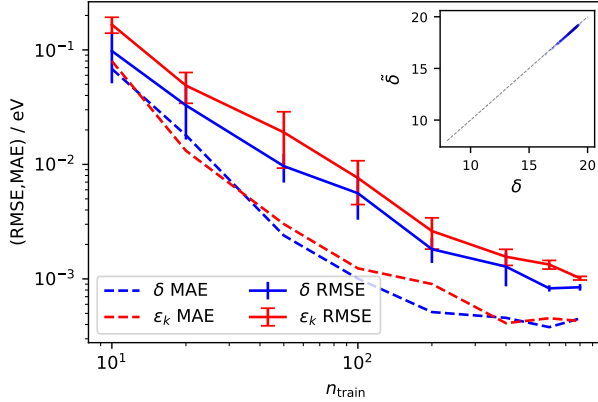


Figure 9: Learning curves for RMSE_ϵ and the HOMO-LUMO gap δ for a test set of 200 water molecules. The curve corresponds to the same predictions as the models trained on the orthogonal $\bar{\mathbf{H}}$ in Fig. 8. The inset shows a parity plot for the predicted versus reference values of δ for $n_{\text{train}} = 800$.

that is obtained by rotating the molecule and swapping the indices of the H atoms. The matrix elements differ, but in a precisely equivariant way: the eigenvalues of the two matrices are identical within machine precision.

We then consider the training of a symmetry-adapted ridge regression model on up to 800 structures, assessing the accuracy of the predictions on up to 200 configurations. The different families of blocks in the Hamiltonian can be learned with compa-

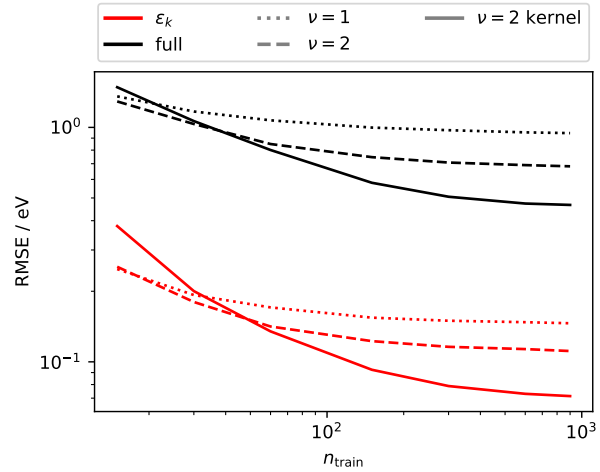


Figure 10: $\text{RMSE}_{\text{full}}$ and RMSE_ϵ for 100 $\text{CH}_3\text{CH}_2\text{OH}$ molecules from the same dataset as in Ref. 37. Different curves correspond to linear models using $\nu = 1, 2$ pair features, and to a SA-GPR model based on $N = 2, \nu = 2$ features.

table accuracy (Fig. 8), with the exception of the antisymmetric combination of off-diagonal (\mathbf{H}, \mathbf{H}) blocks, which contains small entries because most configurations have a near-mirror symmetry. Learning curves show little sign of saturation, despite using a simple linear model, and achieve a $\text{RMSE}_{\text{full}}$ well below 10 meV with a few 100s of configurations. The figure also compares the accuracy of predicting the non-orthogonal Hamiltonian \mathbf{H} , the Löwdin-orthogonalized $\bar{\mathbf{H}}$, and that of estimating the orthogonalized Hamiltonian by applying the exact $\mathbf{S}^{-1/2}$ to the non-orthogonal prediction. Note the error for predicting \mathbf{H} is almost 10 times smaller than that for modeling $\bar{\mathbf{H}}$, but that – even without considering the inconvenience and the further errors connected with predicting or computing the overlap matrix – orthogonalizing the predicted \mathbf{H} increases the error fourfold.

C. Ethanol

We then consider the case of a larger molecule, for which $(N + \nu) = 3$ features cannot provide a full linear basis to learn the matrix elements of the Hamiltonian. We take a random subselection of 1000 Hamiltonian matrices and corresponding structures from the HF/def2-SVP calculations for ethanol in Ref. 37, and further subdivide it into a train set of up to 900 structures and a test set of 100 structures. We build $(N = 1, \nu = 2)$, $(N = 2, \nu = 1)$ and $(N = 2, \nu = 2)$ features starting from neighbor density expansion coefficients with $r_{\text{cut}} = 5 \text{ \AA}$, $\sigma_a = 0.3 \text{ \AA}$, $n_{\text{max}} = 8$, $l_{\text{max}} = 6$, with a data-optimal radial basis and an iterative PCA contraction akin to the NICE scheme to

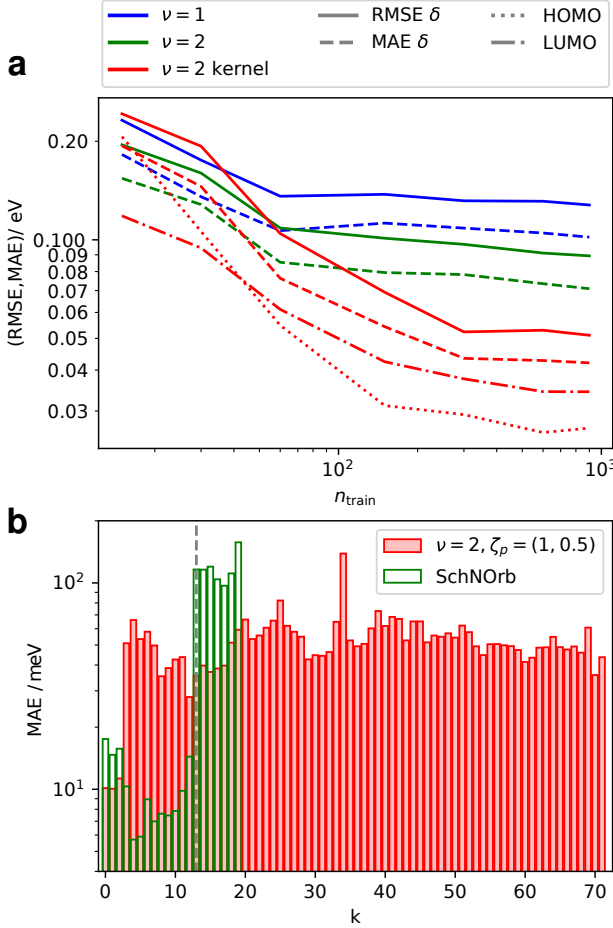


Figure 11: (a) MAE and RMSE for the HOMO-LUMO gap(δ) predictions from linear models using $\nu = 1$ and $\nu = 2$ features. The errors on the prediction and the MAE on the HOMO and LUMO level predictions with kernel models based on $\nu = 2$ features are also plotted. (b) MAE for individual Hamiltonian eigenvalues ϵ_k . Results for the $\nu = 2$ kernel model, with 900 training structures, is compared with the results from SchNOrb³⁷, with 25k training structures.

reduce the number of ($N = 2, \nu = 2$) features.

Linear models based on ($N = 2, \nu = 1$) pair features saturate very early, even though they reach a respectable RMSE_ϵ , below 200 meV on the full spectrum, that spans a range of more than 100 eV (Fig. 10). This is to be expected, as this is a very incomplete description of the pair environments. Increasing the neighbor order to ($N = 2, \nu = 2$) reduces the limiting error by approximately 30%. It is going to a non-linear kernel model, however, that allows to reduce the error to about 70 meV, although the learning curves still approach saturation by $n_{\text{train}} = 900$. We can analyze in more detail the errors for individual electronic levels, and in particular for the HOMO-LUMO gap δ . RMSE and MAE (mean absolute error) follow similar trends as those observed for the overall spectrum, with a substantial improvement seen with the use of

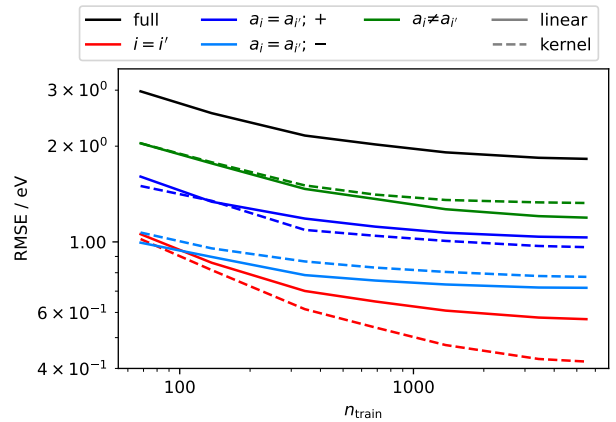


Figure 12: Learning curves for the different blocks of the Fock matrix for the QM7-CHNO dataset. Full and dashed lines correspond to a linear regression and a sparse kernel regression model.

a kernel model, that captures higher body order correlations in the molecular structure (Fig. 11a). Our results for the HOMO (30 meV MAE) and LUMO (40 meV MAE) compare favorably with those reported for SchNOrb (20 and 120 meV), but a direct comparison is not entirely obvious. As shown in Fig. 11b, SchNOrb yields a considerably smaller error for the occupied valence states, but a much larger error for the empty states (at least the 7 energy levels that are shown in Ref. 37). Our model, conversely, yields a relatively constant error across the entire spectrum. Focusing the learning exercise on just a subset of the energy levels might be a good strategy to reduce the error on the orbitals that matter most, but is beyond the scope of the present investigation.

D. Organic molecules

Finally, we turn to the more challenging task of learning the Hamiltonian of a diverse database of organic molecules, containing up to 7 CNO atoms, with different degrees of H saturation.⁵⁰ Even with a small valence basis, this is a task of great complexity, with more than 200 models that have to be trained for the different types of blocks. We choose heuristically a long cutoff $r_{\text{cut}} = 7$ Å, $\sigma_a = 0.3$ Å, and the radial scaling³⁸ $r_0 = 2$ Å, $m = 2$, and generate an optimal radial basis following the procedure in Ref. 41. The large number of different species leads to an explosion of the raw number of features: for the relatively parsimonious density discretization parameters $n_{\text{max}} = 8, l_{\text{max}} = 6$ that we use, the raw number of ($N = 2, \nu = 2$) equivariant features would be in excess of 10^9 per pair. Thus, it becomes essential to perform a data-driven selection, which we implement following the same iterative PCA scheme used for the NICE features in Ref. 40.

As shown in Fig. 12, even a rudimentary linear model (that only describes the dependence of

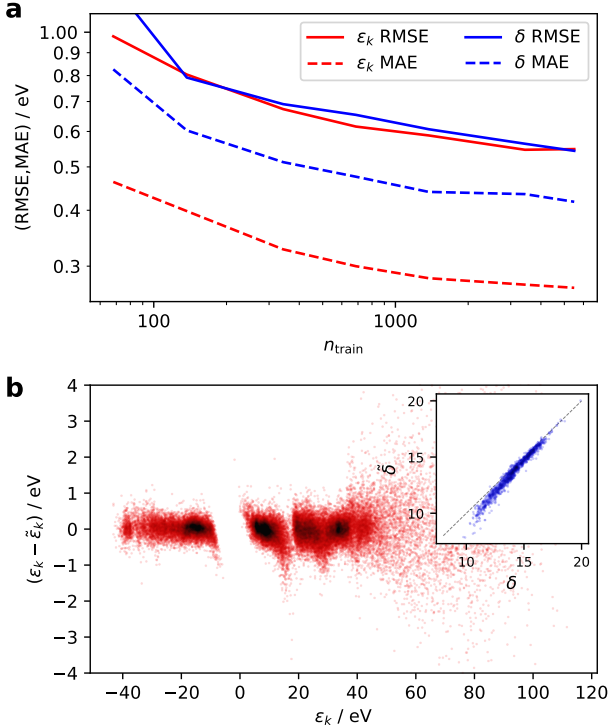


Figure 13: Errors in the prediction of the single-particle energy levels of molecules from the QM7-CHNO dataset. (a) Learning curves for the mean eigenvalue error, and for the error in the HOMO-LUMO gap δ . (b) Signed error in the prediction of electronic eigenvalues ϵ_k as a function of the energy level. Note the larger spread for energies above 40 eV, and for states close to the HOMO-LUMO gap (which is around 0 eV). The inset shows the parity plot for the predicted gap δ .

the matrix elements on 3-body neighbor correlations) achieves rapidly an error that is only three times larger than that we observed for the much simpler case of $\text{CH}_3\text{CH}_2\text{OH}$. It shows however clear signs of saturation, with all the blocks – in particular those corresponding to off-diagonal terms – reaching an almost flat learning curve profile. Moving to a non-linear, $\zeta_p = \{1, 0.1\}$ model delays saturation for the diagonal blocks, but does little for the off-diagonal blocks. We note that the errors appear to be particularly large for molecules containing characteristic molecular motives, such as polyynes and polycycles. We suspect that the high delocalization of the orthogonalized orbitals might be partly to blame, but defer further investigation, as well as the use of higher-order features, to future studies. Similar to what was noted for deep-learning models,³³ the errors for a prediction of the full eigenspectrum are large, with a mean RMSE of 0.6 eV (0.3eV MAE) at the largest train fraction of 80% of the QM7-CHNO dataset. Still, it is worth noting that this is comparable to the accuracy achieved by SchNOrb for the prediction of the full eigenspectrum of $\text{CH}_3\text{CH}_2\text{OH}$ with a large basis (0.48meV MAE)³⁷. In fact, as shown in Fig. 13b, the

high-energy virtual orbitals are predicted with a much larger error than the occupied orbitals, and low-lying excited states. However, given that we use the entire Hamiltonian as a target, the difficult-to-predict high-energy states affect the full range of predictions, and the RMSE in the HOMO-LUMO gap is 0.6 eV RMSE (0.45 eV MAE). This underscores the importance of building models with a loss designed to target only the most relevant part of the information similar to our observations for ethanol.

VI. CONCLUSIONS

We have introduced a construction of symmetry-adapted, atom-permutation and rotation equivariant representations that are suitable to describe quantities associated with multiple atomic centers. The construction is closely related to the density-correlation features that have been used to describe atom-centered environments, and that underlie the vast majority of machine-learning frameworks for the microscopic properties of matter. We propose a practical implementation of the general scheme, that is based on the NICE construction,⁴⁰ but several existing frameworks, including atom-centered symmetry functions,⁴² the atomic cluster expansion,¹⁴ or moment tensor potentials⁸ can be extended along the same lines. It is important to stress that, even if we only show examples for molecular systems, these N -center representations can also be readily applied to the condensed phase.

We then present as an application the construction of machine-learning models of an effective single-particle Hamiltonian, written in an atom-centered basis. Formulating the problem in a fully symmetry-adapted fashion requires manipulating the entries in the Hamiltonian to separate them into blocks with a well-defined behavior with respect to rotation, inversion, particle exchange and Hermitian symmetry. The reward for building a symmetry-adapted model is that, on top of the general symmetries that are explicitly built in, it also automatically incorporates the molecular orbital rules associated with point-group symmetries. We give a striking demonstration of this property by training a model on a random-valued Hamiltonian for a benzene molecule, showing that the *predicted* Hamiltonian yields orbital symmetries that are fully consistent with the expected D_{6h} group characters.

We then benchmark the method on problems of increasing complexity, and find that symmetry-adapted features provide excellent accuracy for homogeneous datasets of distorted H_2O and $\text{CH}_3\text{CH}_2\text{OH}$ molecules – with kernel and linear regression achieving an accuracy comparable to non-symmetry-adapted deep learning models with a fraction of the training set size. Results for a heterogeneous dataset of small organic molecules point to the difficulty of training models for the full Hamiltonian, because of the large errors associated with the virtual orbitals.

From the point of view of building fully equivariant descriptors of N -center atomic clusters, the next challenge will be to introduce higher-body-order terms, with $\nu > 2$, either explicitly or through more sophisticated non-linear models. The general construction we present here provides an easily-extendable framework to do so, as well as to tackle the modeling of 3-center integrals, and higher- N quantities, bringing the full set of ingredients of quantum chemistry calculations within the reach of equivariant machine learning

schemes.

ACKNOWLEDGMENTS

JN and MC acknowledge support by the NCCR MARVEL, funded by the Swiss National Science Foundation (SNSF). We would like to thank Andrea Grisafi and Max Veit for helpful insights and stimulating discussions.

[1] J. Behler and M. Parrinello, *Phys. Rev. Lett.* **98**, 146401 (2007).

[2] A. P. Bartók, M. C. Payne, R. Kondor, and G. Csányi, *Phys. Rev. Lett.* **104**, 136403 (2010).

[3] M. Rupp, A. Tkatchenko, K.-R. Müller, and O. A. von Lilienfeld, *Phys. Rev. Lett.* **108**, 058301 (2012).

[4] V. L. Deringer, A. P. Bartók, N. Bernstein, D. M. Wilkins, M. Ceriotti, and G. Csányi, *Chem. Rev.* **121**, 10073 (2021).

[5] J. Behler, *Chem. Rev.* **121**, 10037 (2021).

[6] A. Bartók, R. Kondor, and G. Csányi, *Physical Review B* **87** (2013).

[7] A. Thompson, L. Swiler, C. Trott, S. Foiles, and G. Tucker, *Journal of Computational Physics* **285**, 316 (2015).

[8] A. V. Shapeev, *Multiscale Model. Simul.* **14**, 1153 (2016).

[9] G. Ferré, T. Haut, and K. Barros, *The Journal of chemical physics* **146**, 114107 (2017).

[10] M. Eickenberg, G. Exarchakis, M. Hirn, and S. Mallasat, *Adv. Neural Inf. Process. Syst.* **2017-Decem**, 6541 (2017).

[11] A. Glielmo, C. Zeni, and A. De Vita, *Phys. Rev. B* **97**, 184307 (2018).

[12] F. A. Faber, A. S. Christensen, B. Huang, and O. A. Von Lilienfeld, *J. Chem. Phys.* **148**, 241717 (2018).

[13] M. J. Willatt, F. Musil, and M. Ceriotti, *J. Chem. Phys.* **150**, 154110 (2019).

[14] R. Drautz, *Phys. Rev. B* **102**, 024104 (2020).

[15] E. Prodan and W. Kohn, *Proc. Natl. Acad. Sci.* **102**, 11635 (2005).

[16] D. M. Grant and R. K. Harris, *Encyclopedia of Nuclear Magnetic Resonance* (J. Wiley & sons, Chichester New York Brisbane, 1996).

[17] C. J. Pickard and F. Mauri, *Phys. Rev. B* **63**, 245101 (2001).

[18] F. M. Paruzzo, A. Hofstetter, F. Musil, S. De, M. Ceriotti, and L. Emsley, *Nat. Commun.* **9**, 4501 (2018).

[19] A. Glielmo, P. Sollich, and A. De Vita, *Phys. Rev. B* **95**, 214302 (2017).

[20] A. Grisafi, D. M. Wilkins, G. Csányi, and M. Ceriotti, *Phys. Rev. Lett.* **120**, 036002 (2018).

[21] B. Anderson, T. S. Hy, and R. Kondor, in *NeurIPS* (2019) p. 10.

[22] O. T. Unke and M. Meuwly, *J. Chem. Theory Comput.* **15**, 3678 (2019).

[23] M. Veit, D. M. Wilkins, Y. Yang, R. A. DiStasio, and M. Ceriotti, *J. Chem. Phys.* **153**, 024113 (2020).

[24] L. Zhang, M. Chen, X. Wu, H. Wang, W. E, and R. Car, *Phys. Rev. B* **102**, 041121 (2020).

[25] D. M. Wilkins, A. Grisafi, Y. Yang, K. U. Lao, R. A. DiStasio, and M. Ceriotti, *Proc. Natl. Acad. Sci. U. S. A.* **116**, 3401 (2019).

[26] A. Grisafi, A. Fabrizio, B. Meyer, D. M. Wilkins, C. Corminboeuf, and M. Ceriotti, *ACS Cent. Sci.* **5**, 57 (2019).

[27] A. Fabrizio, K. R. Briling, D. D. Girardier, and C. Corminboeuf, *J. Chem. Phys.* **153**, 204111 (2020).

[28] S. Yue, M. C. Muniz, M. F. Calegari Andrade, L. Zhang, R. Car, and A. Z. Panagiotopoulos, *J. Chem. Phys.* **154**, 034111 (2021).

[29] A. Grisafi, J. Nigam, and M. Ceriotti, *Chem. Sci.* **12**, 2078 (2021).

[30] K. V. Jose, N. Artrith, and J. Behler, *J. Chem. Phys.* **136**, 194111 (2012).

[31] S. A. Joyce, J. R. Yates, C. J. Pickard, and F. Mauri, *The Journal of Chemical Physics* **127**, 204107 (2007).

[32] A. P. Sutton, A. P. Sutton, M. W. Finnis, D. G. Pettifor, and Y. Ohta, *J. Phys. C Solid State Phys.* **21**, 35 (1988).

[33] J. Westermayr and R. J. Maurer, *Chem. Sci.* **12**, 10755 (2021).

[34] M. Welborn, L. Cheng, and T. F. Miller III, *Journal of chemical theory and computation* **14**, 4772 (2018).

[35] Z. Qiao, M. Welborn, A. Anandkumar, F. R. Manby, and T. F. Miller III, *The Journal of Chemical Physics* **153**, 124111 (2020).

[36] G. Hegde and R. C. Bowen, *Scientific reports* **7**, 1 (2017).

[37] K. T. Schütt, M. Gastegger, A. Tkatchenko, K.-R. Müller, and R. J. Maurer, *Nat Commun* **10**, 5024 (2019).

[38] M. J. Willatt, F. Musil, and M. Ceriotti, *Phys. Chem. Chem. Phys.* **20**, 29661 (2018).

[39] F. Musil, A. Grisafi, A. P. Bartók, C. Ortner, G. Csányi, and M. Ceriotti, *Chem. Rev.* **121**, 9759 (2021).

[40] J. Nigam, S. Pozdnyakov, and M. Ceriotti, *J. Chem. Phys.* **153**, 121101 (2020).

[41] A. Goscinski, F. Musil, S. Pozdnyakov, J. Nigam, and M. Ceriotti, *J. Chem. Phys.* **155**, 104106 (2021).

[42] J. Behler, *The Journal of Chemical Physics* **134**, 074106 (2011).

[43] The coupling relations we write in this section and elsewhere are formally equivalent to the usual relationships that exist for complex-valued spherical harmonics, with the understanding that the CG coefficients need to be adapted accordingly.

[44] A. Grisafi, D. M. Wilkins, M. J. Willatt, and M. Ceriotti, in *Machine Learning in Chemistry*, Vol. 1326, edited by E. O. Pyzer-Knapp and T. Laino (American Chemical Society, Washington, DC, 2019) pp. 1–21.

- [45] H. C. Longuet-Higgins, *Molecular Physics* **6**, 445 (1963).
- [46] E. P. Wigner, *Group theory and its application to the quantum mechanics of atomic spectra* (Academic Press, New York, 1959).
- [47] P. R. Bunker and P. Jensen, *Molecular symmetry and spectroscopy* (NRC research press, 2006).
- [48] H. A. Jahn and E. Teller, *Proceedings of the Royal Society of London. Series A-Mathematical and Physical Sciences* **161**, 220 (1937).
- [49] A. Grisafi, D. M. Wilkins, G. Csányi, and M. Ceriotti, “Dataset: Symmetry-Adapted Machine Learning for Tensorial Properties of Atomistic Systems,” <http://doi.org/10.24435/materialscloud:2018.0009/v1> (2018).
- [50] G. Montavon, M. Rupp, V. Gobre, A. Vazquez-Mayagoitia, K. Hansen, A. Tkatchenko, K. R. Müller, and O. Anatole Von Lilienfeld, *New J. Phys.* **15**, 095003 (2013).
- [51] Q. Sun, X. Zhang, S. Banerjee, P. Bao, M. Barbry, N. S. Blunt, N. A. Bogdanov, G. H. Booth, J. Chen, Z.-H. Cui, *et al.*, *The Journal of chemical physics* **153**, 024109 (2020).
- [52] Q. Sun, T. C. Berkelbach, N. S. Blunt, G. H. Booth, S. Guo, Z. Li, J. Liu, J. D. McClain, E. R. Sayfutyarova, S. Sharma, *et al.*, *Wiley Interdisciplinary Reviews: Computational Molecular Science* **8**, e1340 (2018).